

# Emergence of gravity from quantum field theory in triangulated spacetime and the QFT vector model

Matti Raasakka\*

*Micro and Quantum Systems group, Aalto University, Espoo, Finland*

(Dated: May 13, 2025)

We formulate quantum field theory in triangulated spacetime using compositional quantum field theory and tensor network methods. We show that gravitational interactions emerge as a low-energy effective phenomenon in this framework. For concrete calculations we use free massive scalar field theory in two-dimensional Lorentzian spacetime, but the results generalize to other models and higher dimensions. Finally, our results lead us to propose a new approach to the unification of quantum field theory with gravity, the *QFT vector model*, which combines insights and techniques from various current approaches to quantum gravity such as causal dynamical triangulations, random tensor models, group field theory, emergent gravity and holography.

*Introduction*—Quantum gravity has puzzled physicists for nearly a century by now. Despite a lot of progress on many different approaches [1], the final solution to merging quantum field theory (QFT) with general relativity (GR) remains elusive. The perturbative nonrenormalizability of the QFT model that arises as a direct quantization of GR has prevented the formulation of the fundamental theory of quantum gravity in the same way as for the other fundamental forces of nature [2]. However, this nonrenormalizability may also be taken as a hint towards the effective nature of gravitational phenomena. Indeed, the fundamental nature of gravitational interactions and even spacetime itself has been called into question by various results along the way [3, 4]. As early as 1967 Andrei Sakharov showed that gravitational interactions can emerge as an effective phenomenon from the vacuum fluctuations of matter QFT on curved spacetime [5]—so-called *induced gravity*. This turns out to be a very general result, since the effective action that arises this way consists necessarily of geometric invariants, which at the lowest orders match up exactly in form with the Einstein–Hilbert action for GR [6]. We will follow Sakharov’s lead in this paper as we uncover a similar phenomenon in QFT in triangulated spacetime instead of a continuous one. Our results lead us to propose a new approach to the unification of QFT with gravity—the *QFT vector model*—which combines insights and techniques from various current approaches to quantum gravity such as causal dynamical triangulations, random tensor models, group field theory, emergent gravity and holography.

Triangulated spacetimes are considered in many of the current approaches to quantum gravity, such as causal dynamical triangulations (CDT) [7], spin foams [8], group field theory [9] and random tensor models [10, 11]. In addition to the potential ill-definedness of spacetime geometry below the Planck scale  $l_P = \sqrt{\hbar G/c^3} \sim 10^{-35}$  meters, a practical reason for introducing the triangulation is to make models well-behaved by imposing a high-energy cutoff to the geometric degrees of freedom. Moreover, since the work of Regge [12], it has been understood that GR can be formulated

in a neat coordinate-free way by using triangulated manifolds, thus sidestepping completely the difficult problem of imposing general covariance under coordinate transformations. Curvature—concentrated on codimension-2 faces of the triangulation—is quantified by deficit angles  $\theta_f$ , i.e., the amount of rotation (or, more generally, Lorentz transformation) a gyroscope experiences when going once around the face  $f$ . The Einstein–Hilbert action for GR then takes an intuitive geometric form  $S_{\text{EH}}[\Delta] = (8\pi G)^{-1} \sum_f V_f \theta_f$  for a triangulated manifold  $\Delta$ , where the sum runs over all the faces  $f \in \Delta$ ,  $G$  is the gravitational constant and  $V_f$  the volume of the face  $f$  [13]. (The cosmological constant term, which we neglect in this main article, is discussed in Appendix.) This is taken advantage of, e.g., in CDT and random tensor models [10, 11] to formulate a quantum gravitational path integral over spacetime geometries, where each triangulation is weighted by the amplitude  $e^{iS_{\text{EH}}[\Delta]/\hbar}$ . For us the triangulation will also serve another purpose: Since the gravitational constant  $G$  emerges in our approach as an effective parameter, whose numerical value is computed from the more fundamental description, the discretization scale  $l_\Delta$  of the triangulation (instead of the Planck length  $l_P$ ) determines an absolute length scale.

In the approach we take in this paper the field theory degrees of freedom are not discretized on a lattice, but the continuous fields live in a triangulated spacetime. We will use compositional QFT [14] and tensor network methods [15] to formulate the model first on a single flat  $d$ -simplex—the  $d$ -dimensional generalization of a triangle—and then glue simplices together to obtain QFT amplitudes for more complicated triangulated manifolds. This will give us a general framework for constructing QFT models on piecewise-flat triangulated spacetimes. Importantly, the framework also allows to describe physics inside a spatiotemporally bounded spacetime region. Having the possibility to impose classical geometric boundary data for the bounded region helps with the operational interpretation of the model—especially when we move on to quantum gravity. The boundary can be used to keep track of classical observer time, thus sidestepping

the problem of time(lessness) in quantum gravity [16].

Tensor networks were originally developed as an effective description for ground states of many-body quantum systems, but have since found applications in many different contexts [15]. Our approach draws inspiration from previous works, where tensor networks have been related to spacetime path integrals [17–20] and holography [21, 22]. The basic insight here is that, when quantum amplitudes are expressed as a tensor network contraction, the network structure is reflected in the correlation structure of the amplitudes. On the other hand, for low-energy QFT states the correlation structure closely reflects the geometric structure of the background spacetime due to locality—subsystems with small spatial separation being more correlated than subsystems far apart—thus linking the tensor network structure to spacetime geometry. Following ideas from holography and other works relating entanglement to spacetime structure [23–27], we postulate that fundamentally spacetime structure *is* just an effective description of the correlation structure of the low-energy states of the system [28]. This then implies that *outside* the low-energy regime the QFT boundary amplitudes may not reflect a unique bulk geometry but may be expressed as a linear combination of many different tensor network contraction patterns, leading to a kind of superposition of bulk geometries [29]. We will employ random tensor model techniques to write down a partition function, which generates the sum over all possible QFT tensor network amplitudes compatible with a given boundary data, giving rise to what we call the QFT vector model.

*Methods*—Let us begin the concrete construction of the framework by considering a single  $d$ -simplex  $T$  of linear size  $l_\Delta$  embedded in a flat  $d$ -dimensional Lorentzian spacetime. Following the principles of compositional QFT [14], we associate a quantum state space  $\mathcal{H}_i$  to each boundary  $(d-1)$ -simplex, or *face*,  $F_i \subset \partial T$ , where  $i = 0, \dots, d$  [30]. Let us assume for simplicity that our model consists of a single scalar field, although the construction can be generalized to arbitrary field content. In this case,  $\mathcal{H}_i$  can be constructed as a Fock space by first fixing a basis of functions  $\zeta_k$  in  $L^2(F_i, \mathbb{C})$  ( $k \in \mathbb{N}$ ), the *modes* of the field on the face  $F_i$ . Then  $\mathcal{H}_i$  is linearly spanned by the number states

$$|\mathbf{n}_i\rangle := |n_1^{(i)}, \dots, n_K^{(i)}\rangle \in \mathcal{H}_i, \quad (1)$$

where  $n_k$  is the number of excitations in the mode corresponding to the basis function  $\zeta_k$  and  $K \in \mathbb{N}$ . The *kinematical* state space of the total boundary  $\partial T$  is obtained as the symmetrized tensor product  $\mathcal{H}_{\partial T}^{\text{kin}} = S(\otimes_i \mathcal{H}_i)$ , where  $S$  represents the symmetrization of the boundary excitations according to the statistics of the QFT model. The kinematical boundary state space contains also states, which are not compatible with the dynamics of the model, but these will get removed in the next step.

Next we introduce the amplitude map, which encodes the dynamics of the model by associating probability amplitudes to boundary states [14]. Due to its linearity the amplitude map is an element  $\langle A |$  in the dual space  $(\mathcal{H}_{\partial T}^{\text{kin}})^*$ , and the amplitude for the boundary state  $|\mathbf{n}_0 \dots \mathbf{n}_d\rangle \equiv S(\otimes_i |\mathbf{n}_i\rangle) \in \mathcal{H}_{\partial T}^{\text{kin}}$  is given by  $\langle A | \mathbf{n}_0 \dots \mathbf{n}_d \rangle$ . Concretely, the amplitude can be computed by taking a copy of the corresponding mode function for each boundary excitation, and then integrating over their product using the  $n$ -point function  $G_n$  of the QFT model as the integral kernel. In mathematical notation,

$$\begin{aligned} & \langle A | (\otimes_{i=0}^d |n_1^{(i)}, \dots, n_{K_i}^{(i)}\rangle) \\ &= \left[ \prod_{i=0}^d \prod_{k_i=1}^{K_i} \prod_{m_{k_i}^{(i)}=1}^{n_{k_i}^{(i)}} \int_{F_i} d^{d-1} x_{k_i, m_{k_i}^{(i)}}^{(i)} \zeta_{k_i}(x_{k_i, m_{k_i}^{(i)}}^{(i)}) \right] \\ & \quad \times G_n(x_{1,1}^{(1)}, \dots, x_{K_I, m_{K_I}}^{(I)}), \end{aligned} \quad (2)$$

where  $n = \sum_i \sum_{k_i} n_{k_i}^{(i)}$  is the total number of excitations on the faces. For a flat  $d$ -simplex,  $G_n$  will be the flat spacetime  $n$ -point function, since inside the simplex the physics should be that of flat spacetime according to the equivalence principle. This choice will also guarantee the preservation of local Lorentz symmetry. The *physical* boundary state space is then obtained as  $\mathcal{H}_{\partial T}^{\text{phys}} = P_{\ker A}^\perp \mathcal{H}_{\partial T}^{\text{kin}}$ , where  $P_{\ker A}^\perp$  is the projection onto the orthogonal subspace to the kernel of the amplitude map. This projection gets rid of any unphysical boundary states, which do not respect the dynamics of the model.

We can now think of the amplitudes  $\langle A | \mathbf{n}_1 \dots \mathbf{n}_{d+1} \rangle$  in the Fock basis as tensor components of an infinite-dimensional ‘spacetime tensor’,

$$A_{\mathbf{n}_1 \dots \mathbf{n}_{d+1}} \equiv \langle A | \mathbf{n}_1 \dots \mathbf{n}_{d+1} \rangle. \quad (3)$$

which we will call the *atomic tensor* in our model. We can then obtain amplitudes for any triangulated manifold by contracting a number of atomic tensors according to the geometric structure of the triangulation, because the tensor contraction corresponds to a sum over the Fock basis on a particular face of the triangulation. However, when gluing the atomic tensors together, we have to account for the orientation of the boundaries by introducing the gluing tensor  $G_{\mathbf{n}_1 \mathbf{n}_2}$ , which maps the boundary modes  $\mathbf{n}_1$  on one boundary simplex to the modes  $\mathbf{n}_2$  on the other in a way that implements the change in orientation. (See Fig. 1 for a 2-dimensional example.)

In many cases it may be necessary (or otherwise preferable) to consider several different kinds of simplices, or even other polytopes. The generalization of the above framework is straightforward: We have several different atomic tensors corresponding to the different geometric shapes, which can be contracted along matching faces.

*Results*—We now specialize to the free massive scalar field model in 2d Lorentzian spacetime, allowing us to

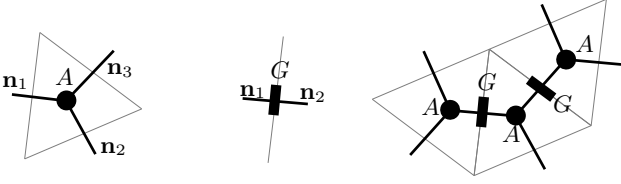


FIG. 1. Left: The graphical representation of the atomic tensor  $A_{n_1 n_2 n_3}$  corresponding to a triangle (gray) as a circle with three legs. Center: The graphical representation of a gluing tensor  $G_{n_1 n_2}$  corresponding to an internal face (gray) of a triangulation as a rectangle with two legs. Right: The graphical representation of a contraction of three atomic tensors, mediated by gluing tensors for the internal faces. Boundary legs carry free indices, which are not marked in the figure.

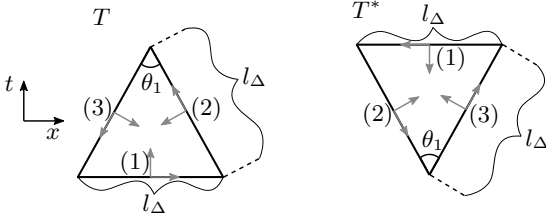


FIG. 2. Two oppositely oriented Lorentzian isosceles triangles  $T$  and  $T^*$  with one spacelike edge (1) and two timelike edges (2) and (3) of proper length/time  $l_\Delta$ . Positive directions on the edges are indicated by arrows.

carry out concrete calculations quite easily. We will discuss the generalization to other models and higher dimensions after presenting the results in this simple case.

In two dimensions a triangulated manifold consists of 2-simplices, i.e., triangles. Similarly to 2d CDT [31], we will consider two oppositely oriented triangles of linear size  $l_\Delta$ , as depicted in Fig. 2, from which more complicated triangulated manifolds can be constructed. Functions of the form  $\zeta_k(s) = e^{2\pi i k s / l_\Delta}$ ,  $k \in \mathbb{Z}$ , form a basis in  $L^2([-l_\Delta/2, l_\Delta/2], \mathbb{C})$  as they satisfy

$$(\zeta_k, \zeta_l) = \int ds \zeta_k(s) \overline{\zeta_l(s)} = l_\Delta^{-1} \delta_{kl}. \quad (4)$$

State spaces on each edge of the triangle are constructed as Fock spaces using  $\zeta_k$  as a basis, as described earlier. The gluing tensor  $G$  maps the modes as  $k \mapsto -k$ , when the edges to be identified are oppositely oriented.

In the free model the  $n$ -point function decomposes into

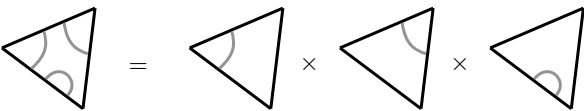


FIG. 3. The decomposition of a multi-particle process amplitude into a product of single-particle process amplitudes.

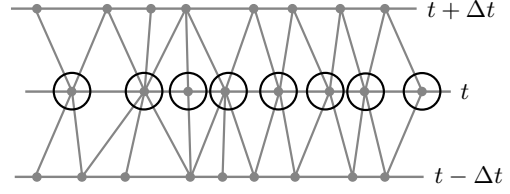


FIG. 4. A portion of a triangulated manifold with three unique equal-time slices at times  $t$  and  $t \pm \Delta t$ . The leading order contribution to the effective low-energy action is given by virtual particle loops around single vertices (in black).

a sum of products of 2-point functions due to Wick's theorem [32]. Thus, an amplitude with  $2n$  boundary excitations can be decomposed into a sum of products of  $n$  amplitudes with two boundary excitations each. The amplitude for any odd number of boundary excitations is zero. (See Fig. 3 for a graphical illustration of the decomposition of one such term.) The amplitude for an excitation in mode  $k$  on edge  $i$  and an excitation in mode  $l$  on edge  $j$  is given by

$$B_{kl}^{(ij)} = \int ds \int ds' \zeta_k(s) \zeta_l(s') G_2(\mathbf{x}^{(i)}(s), \mathbf{x}^{(j)}(s')), \quad (5)$$

where  $G_2$  is the causal two-point function of the model and  $\mathbf{x}^{(i)}(s)$  is the coordinate vector for points on edge  $i$  parametrized by  $s \in [-l_\Delta/2, l_\Delta/2]$ . The amplitudes for the triangles  $T$  and  $T^*$  are equal, since the two triangles are mapped to each other by a spatiotemporal reflection, and the two-point function is invariant under this transformation. Let us call  $B_{kl}^{(ij)}$  the *single-particle process matrices*. The elements  $B_{kl}^{(ij)}$  can be explicitly numerically evaluated up to some mode cutoff  $|k|, |l| \leq n_{\max}$ . They fall off as  $O(|k|^{-1}, |l|^{-1})$ , allowing us to get good numerical estimates for the virtual particle contributions to the amplitudes we are interested in the following. (For numerical analysis we used the values  $l_\Delta = 1$ ,  $m = 1$  and  $n_{\max} = 50$ . See Appendix for details.) We used the SciPy Python library [33] for numerical computations. Our Python scripts can be found at [34].

Now consider for example a portion of a triangulated manifold such as illustrated in Fig. 4. Such triangulations with unique equal-time slices are considered in CDT. We are interested in the amplitude between the equal-time slices at  $t \pm \Delta t$ , which we obtain by contracting the atomic tensors using the gluing tensor according to the structure of the triangulation. If we are interested in the low-energy behavior of the model, we can derive the *effective low-energy action* for the model by summing over high-energy degrees of freedom up to some cutoff scale  $\Lambda$  [2]. Since the lowest non-zero mode  $\zeta_1$  on an edge has wavelength  $\sim l_\Delta$ , we can implement the sum over high-energy degrees of freedom by setting the triangulation length scale to  $l_\Delta = 1/\Lambda$  and summing over all modes except for

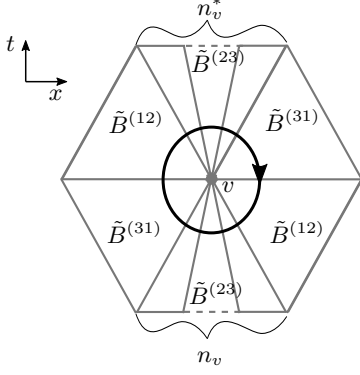


FIG. 5. One virtual particle loop around a single vertex  $v$  of the triangulation with  $n_v$  triangles  $T$  to the past of  $v$  and  $n_v^*$  triangles  $T^*$  to the future. The amplitude is obtained by contracting the single-particle process matrices with the gluing tensor according to the connectivity of the triangles.

$k = 0$ . The leading order contribution to the amplitude comes from virtual particle loops around single vertices of the triangulation at the intermediate time  $t$ , such as illustrated in Fig. 4. Let us denote by  $\tilde{G} \equiv \delta_{k,-k}$  and  $\tilde{B}$  the gluing and single-particle process matrices with the zero mode removed. Then, the multiplicative contribution  $A_v$  to the full amplitude given by one such vertex loop around the vertex  $v$ , as in Fig. 5, is given by

$$\text{tr}((\tilde{G}\tilde{B}^{(23)})^{n_v}\tilde{G}\tilde{B}^{(31)}\tilde{G}\tilde{B}^{(12)}(\tilde{G}\tilde{B}^{(23)})^{n_v^*}\tilde{G}\tilde{B}^{(31)}\tilde{G}\tilde{B}^{(12)}),$$

where  $n_v$  is the number of  $T$  triangles to the past of  $v$  and  $n_v^*$  is the number of  $T^*$  triangles to the future of  $v$ . Due to the fact that the  $\tilde{B}^{(23)}$  matrix elements are dominated by the lowest order modes,  $\tilde{G}\tilde{B}^{(23)}$  has one dominating eigenvalue  $\sigma$ , which is more than twice as large as the next largest. Thus, we can approximate

$$A_v \approx C\sigma^{n_v+n_v^*}, \quad (6)$$

where  $C$  is some constant independent of  $n_v$  and  $n_v^*$ . By a direct numerical evaluation we find that the complex phase of  $A_v$  is closely proportional to  $e^{i\Delta\varphi(n_v+n_v^*)}$ , where  $\Delta\varphi \approx 2.6$ , with some deviation for  $n_v, n_v^* < 3$ . (See Fig. 6.) This behavior of the phase angle can be interpreted as the gravitational Aharonov–Bohm effect [35], where the amplitude of a virtual particle picks up an additional phase when going around a region with non-zero curvature. In our case, the approximately linear behavior of the phase angle produces an effective gravitational amplitude of the correct form  $e^{iS_{\text{EH}}[\Delta]}$ , since the number of triangles  $n_v + n_v^*$  is related linearly to the deficit angle:

$$\theta_v = (2 - n_v - n_v^*)\theta_1, \quad (7)$$

where  $\theta_1 = \text{arccosh}(\frac{3}{2}) \approx 0.96$  is the hyperbolic angle opposite to edge (1) in triangle  $T$ . In 2d we have  $S_{\text{EH}}[\Delta] = -\frac{1}{8\pi G} \sum_{v \in \Delta} \theta_v$ , where the summation runs

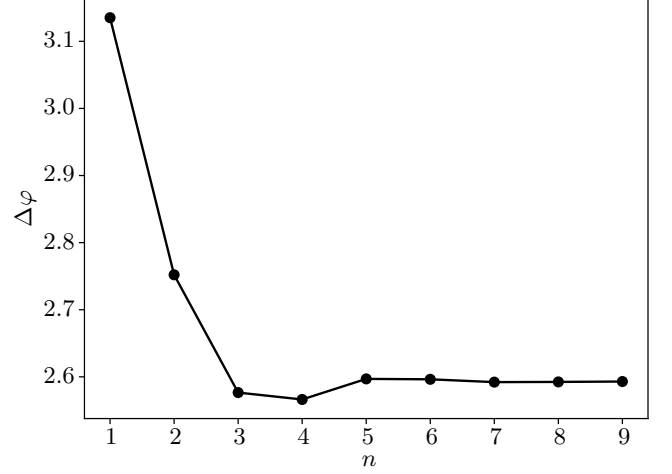


FIG. 6. The difference in the complex phase angle  $\Delta\varphi$  of the vertex loop amplitude  $A_v$  between consecutive values of  $n$  as a function of  $n$  with fixed  $n^* = 0$ . The dependence is similar for other values of  $n^*$ . The difference  $\Delta\varphi$  converges to a constant, indicating an approximately linear dependence of the phase angle on  $n$  for  $n > 2$ . Since the amplitude is symmetric with respect to  $n$  and  $n^*$ , the same conclusion applies to  $n^*$ .

over all the vertices in  $\Delta$ . (Notice that timelike deficit angles around spacelike faces contribute negatively to the action [13]. The volume of a vertex is set to 1 following [7].) Accordingly,

$$e^{iS_{\text{EH}}[\Delta]} = \prod_v e^{\frac{i}{8\pi G}(n_v+n_v^*)\theta_1}, \quad (8)$$

which matches in form the contribution  $\prod_v e^{i\Delta\varphi(n_v+n_v^*)}$  to the amplitude from the vertex loops. Equating the numerical factors gives value  $G_{\text{eff}} = \frac{\theta_1}{8\pi\Delta\varphi} \approx 0.015$  to the effective gravitational constant. We have thus demonstrated the emergence of effective low-energy gravitational interactions from the QFT vacuum fluctuations in free scalar field model in 2d triangulated spacetime.

Of course, the simple model we considered above is far from realistic, and one can only hope to achieve a qualitative agreement with reality. The two-dimensional case is somewhat special, since in 2d the gravitational constant is dimensionless. In higher dimensions, spacetime curvature is concentrated on the codimension-2 faces of the triangulation. Just as in the 2d case, the amplitudes for the virtual particle loops around the codimension-2 faces give rise to a low-energy effective gravitational action due to the gravitational Aharonov–Bohm effect. In particular, in 4d the volume of the faces will be proportional to  $l_\Delta^2$ , linking the discretization scale to the magnitude of the effective gravitational constant  $G_{\text{eff}} \propto l_\Delta^2$ . If the discretization scale is set to around Planck length, we obtain the observed magnitude for the gravitational constant. Moreover, if we consider a model with several different fields, each field contributes with its own loop



amplitude to the effective gravitational action. Nevertheless, the overall mechanism for the emergence of gravity from high-energy QFT vacuum fluctuations remains intact also for more realistic models. However, we leave the detailed analysis of these models to future work.

*QFT vector model*—Thus far we have shown that high-energy QFT vacuum fluctuations in triangulated spacetime give rise to an effective low-energy gravitational action. Consequently, we do not need to include gravitational dynamics explicitly into the fundamental model in order to obtain a unified theory of quantum matter and gravity. Now we proceed to apply these insights into formulating a new approach to quantum gravity.

In the previous sections we only considered situations where the triangulated background spacetime had a definite geometric structure. In order to obtain a model for quantum gravity, we need to allow for superpositions of different spacetime structures—and eventually sum over all possible geometries, which are compatible with the given boundary data. In our framework this means that we no longer have just one tensor network for the boundary amplitude. Instead, the amplitude is obtained as a linear combination of many different tensor networks. This implies that the correlations in the boundary amplitudes no longer reflect a unique bulk spacetime structure.

The sum over tensor network amplitudes corresponding to different bulk spacetimes could be implemented as in CDT by numerically summing over the different discretizations. However, it can also be mathematically expressed using a generating function similarly to random tensor models [11] and group field theory [9]. Again, for concreteness, consider the 2d scalar field model from previous section. In the model we have two kinds of edges, spacelike and timelike, and two kinds of triangles  $T$  and  $T^*$  giving rise to the atomic tensors  $A_{\mathbf{n}_1\mathbf{n}_2\mathbf{n}_3}^{(T)}$  and  $A_{\mathbf{n}_1\mathbf{n}_2\mathbf{n}_3}^{(T^*)}$ . Denote the state space on a single spacelike edge by  $\mathcal{H}_s$  and on a single timelike edge by  $\mathcal{H}_t$ . Now consider the action functional

$$S[\Psi_{\mathbf{n}}^{(i)}; \lambda] = \frac{1}{2} \sum_{i=s,t} G_{\mathbf{n}_1\mathbf{n}_2}^{-1} \Psi_{\mathbf{n}_1}^{(i)} \Psi_{\mathbf{n}_2}^{(i)} + \frac{\lambda}{2} \sum_{j=T, T^*} A_{\mathbf{n}_1\mathbf{n}_2\mathbf{n}_3}^{(j)} \Psi_{\mathbf{n}_1}^{(s)} \Psi_{\mathbf{n}_2}^{(t)} \Psi_{\mathbf{n}_3}^{(t)}, \quad (9)$$

where repeated Fock space indices  $\mathbf{n}_k$  are summed over, and  $\Psi_{\mathbf{n}}^{(i)}$  ( $i = s, t$ ) are state vectors on spacelike and timelike edges—the dynamical variables in this action.  $G_{\mathbf{n}_1\mathbf{n}_2}^{-1}$  is the inverse gluing tensor giving rise the quadratic terms in the action.  $A_{\mathbf{n}_1\mathbf{n}_2\mathbf{n}_3}^{(j)}$  ( $j = T, T^*$ ) are the atomic tensors corresponding to the triangles  $T$  and  $T^*$ , which give rise to the cubic interaction terms. Finally,  $\lambda$  is a coupling constant. Then, the partition function

$$Z(\lambda) = \int \left[ \prod_{i=s,t} d\Psi^{(i)} \right] e^{-S[\Psi^{(i)}; \lambda]} \quad (10)$$

gives rise to a random vector model based on the previous QFT model on triangulated spacetime. This partition function defines the *QFT vector model*. Similarly to random tensor models [11] and group field theory [9], the diagrams arising from the Feynman expansion of  $Z(\lambda)$  in powers of  $\lambda$  correspond exactly to all closed triangulated manifolds, which are obtained by gluing triangles  $T$  and  $T^*$  together along either spacelike or timelike edges. The Feynman rules for computing the amplitudes consist of inserting one atomic tensor for each interaction vertex (i.e., a triangle), whose indices are contracted with the gluing tensor according to the structure of the manifold. Thus, the Feynman amplitudes reproduce exactly the amplitudes for QFT in triangulated spacetime we considered in the previous section, except weighted by  $\lambda^{N_t}/\Sigma_\Delta$  where  $N_t$  is the number of triangles in the triangulation and  $\Sigma_\Delta$  is a symmetry factor for the Feynman diagram. Accordingly, the partition function contains the full non-perturbative model, which is obtained by summing over the amplitudes for all possible triangulated manifolds. Moreover, the proportionality of amplitudes to  $\lambda^{N_t}$  allows to renormalize the effective cosmological constant by scaling the QFT vector model coupling constant  $\lambda$ . (See Appendix for more discussion on the effective cosmological constant.)

Amplitudes for boundary states can be expressed as expectation values in the QFT vector model. Consider a spacetime region  $R$ , whose boundary  $\partial R$  consists of  $N$  edges. The kinematical boundary state space is then given by  $\mathcal{H}_{\partial R}^{\text{kin}} = S(\otimes_{k=1}^N \mathcal{H}_{i_k})$ , where  $i_k \in \{s, t\} \forall k$  and  $S$  denotes the appropriate symmetrization. Let  $\chi_{\mathbf{n}_1 \dots \mathbf{n}_N}$  be the components of a boundary state  $|\chi\rangle \in \mathcal{H}_{\partial R}^{\text{kin}}$ . Then the quantum gravitational QFT vector model amplitude for this boundary state is given by

$$A(\chi_{\mathbf{n}_1 \dots \mathbf{n}_N}; \lambda) = \frac{1}{Z(\lambda)} \int \left[ \prod_{i=s,t} d\Psi^{(i)} \right] \left[ \prod_{k=1}^N G_{\mathbf{m}_k\mathbf{n}_k} \right] \left[ \prod_{k=1}^N \Psi_{\mathbf{m}_k}^{(i_k)} \right] \times \chi_{\mathbf{n}_1 \dots \mathbf{n}_N} e^{-S[\Psi^{(i)}; \lambda]}. \quad (11)$$

The dynamical fields  $\Psi_{\mathbf{m}_k}^{(i_k)}$  in the tensor contraction act as sources, coupling the boundary field  $\chi_{\mathbf{n}_1 \dots \mathbf{n}_N}$  to the bulk dynamics. The integration results in a sum over all amplitudes corresponding to bulk geometries, which are compatible with the boundary data.

It is interesting to note that the high-energy regime of the 2d scalar QFT vector model resembles random matrix models of the kind that have been previously linked to 2d quantum gravity [10]. This is the regime where each boundary edge has exactly two excitations—the components  $M_{kl}$  of a two-particle edge state  $M_{kl}|kl\rangle \in \mathcal{H}_i$ , where  $|kl\rangle$  is a state with one excitations in each mode  $k$  and  $l$ , acting as a random matrix. Intriguingly, this is also the regime where the leading order effective gravitational terms arise to the action. However, the full QFT

vector model is much richer than a simple matrix model, of course, and the degrees of freedom have a clear physical interpretation unlike in random matrix models.

QFT vector models corresponding to other QFT models and higher dimensions can also be defined in exactly the same way as in the case of 2d scalar field. We leave the further exploration of these models to future work.

*Summary*—To conclude, let us summarize our results. We first developed a theoretical framework, based on compositional QFT and tensor network methods, for studying QFT in triangulated spacetime. We then showed that the high-energy vacuum fluctuations in free massive scalar QFT in 2d triangulated spacetime give rise to an effective low-energy gravitational action, and pointed out the generalization of these results to more realistic models. Finally, we introduced the QFT vector model as a unified model for quantum matter and gravity, in which the effective quantum gravitational amplitudes arise from the high-energy vacuum fluctuations of the matter fields, thus removing the need to explicitly introduce gravitational dynamics.

Our work opens up several new avenues of research. Studying in more detail the emergence of low-energy effective gravitational dynamics in more realistic QFT models in 4d will be the necessary first step in bridging the gap to reality. However, the 2d QFT vector model also warrants further investigation. It would be interesting to see if the successes of 2d matrix models and CDT in reproducing reasonable macroscopic spacetime geometries can be achieved also in this model. Other interesting questions include, e.g., the fate of unitarity in non-trivial and superposed spacetime geometries. Finally, the exact formulation and study of QFT vector models for more realistic QFT models (e.g., incorporating fermions and local gauge symmetry) is essential to see if the approach can in fact successfully merge QFT and gravity.

*Acknowledgments*—We acknowledge the computational resources provided by the Aalto Science-IT project.

## Appendix

*Numerical evaluation of single-particle process matrices*—Here we present the explicit numerical evaluation of the single-particle process matrices  $B^{(ij)}$  for free massive scalar field theory in 2d Lorentzian spacetime.

We consider two oppositely oriented flat Lorentzian isosceles triangles  $T$  and  $T^*$ , as explained in the main text. (See Fig. 2.) The boundary of  $T$  consists of three boundary edges  $e_i \subset \partial T$ ,  $i = 1, 2, 3$ , so that  $\partial T = \cup_i e_i$ , and similarly for  $T^*$ . Each edge has proper length/time  $l_\Delta > 0$ . The intersections of the edges are the vertices of the triangle,  $e_i \cap e_j = v_k$ ,  $k = 1, 2, 3$  s.t.  $k \neq i, j$ . The points on the edges of  $T$  are given by the 2-vectors  $x^{(i)} = st^{(i)} + l_\Delta c^{(i)}$ , where  $s \in [-l_\Delta/2, l_\Delta/2]$  parametrizes

the points,  $t^{(i)}$  is the tangent vector to the edge  $(i)$ , and  $l_\Delta c^{(i)}$  is the center of the edge  $(i)$ . Explicitly, we choose the triangle to have its base (edge (1)) on the  $x$ -axis and be symmetric with respect to the  $t$ -axis, giving

$$t^{(1)} = (0, 1), \quad c^{(1)} = (0, 0), \quad (12)$$

$$t^{(2)} = (\sqrt{5}/2, -1/2), \quad c^{(2)} = (\sqrt{5}/4, 1/4), \quad (13)$$

$$t^{(3)} = (-\sqrt{5}/2, -1/2), \quad c^{(3)} = (\sqrt{5}/4, -1/4). \quad (14)$$

The edge vectors for  $T^*$  are obtained via spacetime reflection as  $-x^{(i)}(s)$ .

An orthogonal basis of functions on each edge is given by the functions

$$\zeta_k(s) = \frac{1}{l_\Delta} e^{i2\pi \frac{k}{l_\Delta} s}, \quad k \in \mathbb{Z},$$

where again  $s \in [-\frac{l_\Delta}{2}, \frac{l_\Delta}{2}]$  is the coordinate labeling points along the edge. (Note that  $\zeta_{-k} = \overline{\zeta_k}$ .) The normalization is chosen such that they satisfy the orthogonality relation

$$(\zeta_k, \zeta_l) = \int_{[-\frac{l_\Delta}{2}, \frac{l_\Delta}{2}]} ds \overline{\zeta_k(s)} \zeta_l(s) = \frac{1}{l_\Delta} \delta_{kl},$$

which approaches the Dirac delta in the continuum limit  $l_\Delta \rightarrow 0$ . Also, with this normalization the amplitudes come out dimensionless, which is important.

The causal two-point function (i.e., Feynman propagator) of the free self-adjoint scalar field is defined as

$$\begin{aligned} G_2(x, y) &= -i \langle 0 | T \hat{\phi}(x) \hat{\phi}(y) | 0 \rangle \\ &= -i \begin{cases} \langle 0 | \hat{\phi}(x) \hat{\phi}(y) | 0 \rangle & \text{if } x_0 \geq y_0, \\ \langle 0 | \hat{\phi}(y) \hat{\phi}(x) | 0 \rangle & \text{if } x_0 < y_0, \end{cases} \end{aligned} \quad (15)$$

where  $T$  denotes the time-ordering. Using standard methods, this can be expressed as [32]

$$G_2(x, y) = -i \int_{\mathbb{R}} \frac{dp_1}{4\pi p_0} e^{-\text{sgn}(x_0 - y_0) i p \cdot (x - y)}, \quad (16)$$

where  $p_0 = \sqrt{p_1^2 + m^2}$ ,  $p = (p_0, p_1)$ , and ‘sgn’ denotes the sign function. The elements of the single-particle process matrix  $B^{(ij)}$  can then be generally expressed as

$$B_{kl}^{(ij)} = \int_{-\frac{l_\Delta}{2}}^{\frac{l_\Delta}{2}} ds \int_{-\frac{l_\Delta}{2}}^{\frac{l_\Delta}{2}} ds' \zeta_k(s) \zeta_l(s') G_2(x^{(i)}(s), x^{(j)}(s')).$$

Substituting the expressions for the basis functions  $\zeta_k$  and the two-point function  $G_2$ , the integrals over the parameters  $s$  and  $s'$  can be carried out analytically. We note that  $B_{kl}^{(ji)} = B_{lk}^{(ij)}$ . Furthermore, the neutral scalar field two-point function is symmetric under spacetime reflection (i.e., a  $PT$ -transformation),  $G_2(-x, -y) = G_2(x, y)$ , so the amplitudes for  $T$  and  $T^*$  are equal.

The explicit expressions for the  $B$  matrix elements are as follows:

$$B_{kl}^{(1j)} = -i \int_{\mathbb{R}} \frac{dp_1}{4\pi p_0} e^{ip \cdot (c^{(1)} - c^{(j)})l_{\Delta}} F_k(-p \cdot t^{(1)} \frac{l_{\Delta}}{2}) F_l(p \cdot t^{(j)} \frac{l_{\Delta}}{2}) \quad \forall j = 1, 2, 3, \quad (17)$$

$$B_{kl}^{(22)} = \int_{\mathbb{R}} \frac{dp_1}{8\pi p_0} \left[ K_{kl}^{(2)}(p) - \overline{K_{kl}^{(2)}(-p)} \right], \quad (18)$$

$$B_{kl}^{(33)} = \int_{\mathbb{R}} \frac{dp_1}{8\pi p_0} \left[ K_{kl}^{(3)}(-p) - \overline{K_{kl}^{(3)}(p)} \right], \quad (19)$$

$$B_{kl}^{(23)} = \int_{\mathbb{R}} \frac{dp_1}{8\pi p_0} \left[ e^{-ip \cdot (c^{(2)} - c^{(3)})l_{\Delta}} L_{kl}^{(23)}(p) - e^{ip \cdot (c^{(2)} - c^{(3)})l_{\Delta}} \overline{L_{kl}^{(23)}(-p)} \right], \quad (20)$$

where the various special functions are

$$\begin{aligned} F_k(q) &= \frac{\sin(\pi k - q)}{\pi k - q}, \\ K_{kl}^{(i)}(p) &= \frac{\delta_{k,-l} - F_k(-p \cdot t^{(i)} \frac{l_{\Delta}}{2}) e^{i(\pi l - p \cdot t^{(i)} \frac{l_{\Delta}}{2})}}{\pi l - p \cdot t^{(i)} \frac{l_{\Delta}}{2}}, \\ L_{kl}^{(ij)}(p) &= \frac{F_{k-l}(p \cdot (t^{(i)} + t^{(j)}) \frac{l_{\Delta}}{2}) - F_k(p \cdot t^{(i)} \frac{l_{\Delta}}{2}) e^{i(\pi l + p \cdot t^{(j)} \frac{l_{\Delta}}{2})}}{\pi l + p \cdot t^{(j)} \frac{l_{\Delta}}{2}}. \end{aligned}$$

At the special points  $p \cdot t^{(i)} \frac{l_{\Delta}}{2} = \pm k, \pm l$  some of the denominators of the integrands for  $B_{kl}^{(ij)}$  go to zero. Even though the integrands themselves are in fact well-behaved differentiable functions at these points, they still need to be treated separately in the numerical implementation, e.g., by setting the value of the function to the limiting value close to the special point. With that taken care of, the integrals for  $B_{kl}^{(ij)}$  can be numerically evaluated using standard numerical packages. We used the ‘quad’ integrator in the SciPy Python package [33]. The code we used for evaluating the  $B$  matrix elements can be found at [34]. Evaluating one  $B$  matrix up to a mode cutoff  $|k|, |l| \leq 50$  on one CPU core took up to  $\sim 40$  minutes, but the code could definitely be optimized further, e.g., via parallelization.

*Discrete gravity action*—Next we describe some details of the discretization of GR following mostly the exposition in [13]. The continuum Einstein-Hilbert action in  $d$ -dimensional Lorentzian spacetime with metric signature  $(+, -, \dots, -)$  reads

$$S_{EH}[g] = \frac{1}{2\kappa} \int_{\mathcal{M}} d^d x \sqrt{|\det g|} (R - 2\Lambda),$$

where  $\kappa = 8\pi G/c^4$ ,  $G$  is the gravitational constant,  $\Lambda$  the cosmological constant,  $R$  is the (Ricci) scalar curvature, and  $g$  denotes the spacetime metric. We integrate over the whole spacetime manifold  $\mathcal{M}$ . (Here we assume for simplicity that  $\mathcal{M}$  does not have a boundary. In the case of a non-empty boundary the action would contain additional boundary terms.) In the  $d = 2$  case, we discretize spacetime by considering triangulations with flat triangles  $T$  and  $T^*$  as discussed in the main text. Curvature of the triangulated manifold is concentrated on codimension-2 subsimplices, which in the 2d case are the

0-dimensional vertices. A closed loop around a single vertex is timelike, and the non-trivial holonomy around the loop is a 2d Lorentz boost given by the coordinate transformation

$$\begin{aligned} t' &= \cosh(\theta_v) t - \sinh(\theta_v) x, \\ x' &= \cosh(\theta_v) x - \sinh(\theta_v) t, \end{aligned}$$

where  $\theta_v$  is a hyperbolic deficit angle, which quantifies the curvature at the vertex  $v$  [12, 13]. The Einstein-Hilbert action for the triangulated manifold can then be written as

$$S_{EH} = \frac{1}{\kappa} \left[ \sum_v V_v \theta_v - V_{\Delta} \Lambda \right],$$

where  $V_v$  is the volume of a single vertex, and  $V_{\Delta}$  is the spacetime volume of the triangulation. We set  $V_v \equiv 1$  following the convention in [7]. Notice also that the sign of the contribution to the For the total spacetime volume of the triangulation we obviously have  $V_{\Delta} = N_t V_t$ , where  $N_t$  is the number of triangles in the triangulation and  $V_t$  the volume of a single triangle.

In two spacetime dimensions the integral over the curvature leads in fact to a purely topological term [31], which would allow us to further simplify the form of the action. However, we keep the curvature term explicit in our analysis, since this is the form that arises naturally from the virtual particle loops. Moreover, it also helps us to see how our results in 2d would generalize to higher dimensions, where GR is no longer topological. The unsimplified form of the action generalizes in a straightforward manner to higher dimensions, where the sum still runs over all the codimension-2 subsimplices with deficit angles quantifying the curvature. As

in the 2d case, the deficit angles are again related to the Aharonov-Bohm phase shifts of virtual particle loops around the codimension-2 subsimplices.

*Cosmological constant*—The main challenge for the original induced gravity proposal of Sakharov [5] was to reproduce the observed value for the cosmological constant [6]. Indeed, as is well-known, the effective cosmological constant arising from continuum QFT vacuum fluctuations comes out as dozens of orders of magnitude too large—the infamous ‘worst prediction in the history of physics’. Therefore, it is crucial to examine if the framework we introduced can help with this problem.

There are at least two ways we can get around the problem: (i) By considering microscopic QFT models for which the contributions to the effective cosmological constant from bosonic and fermionic degrees of freedom (nearly) cancel out, since these contribute with opposite signs. (ii) As noted in the main text, the effective cosmological constant can be renormalized in the QFT vector model by scaling the QFT vector model coupling constant  $\lambda$ , since the QFT vector model Feynman amplitudes are proportional to  $\lambda^V$ , where  $V$  is the total spacetime volume. The running of  $\lambda$  as a function of the renormalization scale can then be studied. This cures the cosmological constant problem in the QFT vector model. However, further investigation is certainly needed in order to fill in the technical details.

With the above general remarks in mind, in the rest of this section we concentrate on the numerical evaluation of the leading order contributions to the effective cosmological constant in the 2d free scalar field model. These arise from virtual single-particle loops crossing over only one edge. The contribution to the amplitude coming from a loop crossing the spacelike edge (1) is real-valued, so it does not contribute to the effective cosmological constant. Both timelike edges (2) and (3) contribute to the amplitude a factor

$$\text{tr}(\tilde{G}\tilde{B}^{(ii)}\tilde{G}\tilde{B}^{(ii)}) \propto e^{i\gamma}, \quad (21)$$

where  $\gamma \approx 3.1$ . Since each edge is shared by two triangles, and each triangle has two timelike edges, this is also the leading order contribution by one triangle to the effective cosmological constant. The cosmological constant term in the gravitational action can be written as

$$e^{\frac{i}{\kappa}\Lambda V_t N_t} = \prod_{t=1}^{N_t} e^{\frac{i}{\kappa}\Lambda V_t}, \quad (22)$$

where the product runs over all the triangles in the triangulation. Thus, equating the factor  $e^{\frac{i}{\kappa}\Lambda V_t}$  arising from one triangle with the phase of the loop amplitude  $e^{i\gamma}$ , we get for the effective cosmological constant  $\Lambda_{\text{eff}} = \frac{\kappa_{\text{eff}}}{V_t}\gamma$ , where  $\kappa_{\text{eff}} = 8\pi G_{\text{eff}}$  and  $G_{\text{eff}} = \frac{\theta_1}{8\pi\Delta\varphi} \approx 0.015$  is the effective gravitational constant evaluated in the main text. The volume of a single triangle ( $T$  or  $T^*$ ) is

given by  $V_t = \frac{\sqrt{5}}{2}l_\Delta^2$ . Substituting everything in, we get  $\Lambda_{\text{eff}} = \frac{16\pi G_{\text{eff}}\gamma}{\sqrt{5}}l_\Delta^{-2} \approx 1.0 l_\Delta^{-2}$ . Thus, the effective cosmological constant comes out the same order of magnitude as  $l_\Delta^{-2}$ , and diverges in the continuum limit  $l_\Delta \rightarrow 0$ —as could have been expected from the continuum theory.

---

\* matti.raasakka@aalto.fi

- [1] D. Oriti, ed., *Approaches to Quantum Gravity* (Cambridge University Press, 2009).
- [2] C. P. Burgess, Quantum gravity in everyday life: General relativity as an effective field theory, *Living Rev Rel* **7** (2004).
- [3] T. Jacobson, Thermodynamics of spacetime: The Einstein equation of state, *Phys Rev Lett* **75**, 1260–1263 (1995), arXiv:gr-qc/9504004.
- [4] E. Verlinde, On the origin of gravity and the laws of Newton, *JHEP* **2011** (4), arXiv:1001.0785 [hep-th].
- [5] A. Sakharov, Vacuum quantum fluctuations in curved space and the theory of gravitation, *Sov Phys Dokl* **12**, 1040 (1968), reprinted in *Gen Rel Grav* **32**, 365–367 (2000).
- [6] M. Visser, Sakharov’s induced gravity: A modern perspective, *Mod Phys Lett A* **17**, 977 (2002), arXiv:gr-qc/0204062.
- [7] J. Ambjørn, J. Jurkiewicz, and R. Loll, Dynamically triangulating Lorentzian quantum gravity, *Nucl Phys B* **610**, 347–382 (2001).
- [8] A. Perez, The spin-foam approach to quantum gravity, *Living Rev Rel* **16** (2013).
- [9] D. Oriti, The group field theory approach to quantum gravity, in *Approaches to Quantum Gravity*, edited by D. Oriti (Cambridge University Press, 2009) pp. 310–331, arXiv:gr-qc/0607032.
- [10] P. Di Francesco, P. Ginsparg, and J. Zinn-Justin, 2d gravity and random matrices, *Phys Rep* **254**, 1 (1995), arXiv:hep-th/9306153.
- [11] R. Gurau and V. Rivasseau, Quantum gravity and random tensors (2024), arXiv:2401.13510 [hep-th].
- [12] T. Regge, General relativity without coordinates, *Il Nuovo Cimento* **19**, 558 (1961).
- [13] R. Sorkin, Time-evolution problem in Regge calculus, *Phys Rev D* **12**, 385 (1975), erratum published in *Phys Rev D* **23**, 565 (1981).
- [14] R. Oeckl and J. Orendain Almada, Compositional quantum field theory: An axiomatic presentation, *J Math Phys* **65** (2024), arXiv:2208.10385 [hep-th].
- [15] R. Orús, Tensor networks for complex quantum systems, *Nature Rev Phys* **1**, 538–550 (2019).
- [16] R. Oeckl, Schrödinger’s cat and the clock: lessons for quantum gravity, *Class Quant Grav* **20**, 5371–5380 (2003).
- [17] A. May, Tensor networks for dynamic spacetimes, *JHEP* **2017** (6), arXiv:1611.06220 [hep-th].
- [18] A. Milsted and G. Vidal, Tensor networks as path integral geometry (2018), arXiv:1807.02501 [cond-mat.str-el].
- [19] Z. Yang, A. Bhattacharyya, L. Cheng, L.-Y. Hung,



- and S. Ning, Emergent Lorentz symmetry and the Unruh effect in a Lorentzian fermionic tensor network, *Phys Rev D* **99**, 086007 (2019).
- [20] J. F. Pedraza, A. Russo, A. Svesko, and Z. Weller-Davies, Computing spacetime, *Int J Mod Phys D* **31** (2022), arXiv:2205.05705 [hep-th].
- [21] B. Swingle, Constructing holographic spacetimes using entanglement fundamentalization (2012), arXiv:1209.3304 [hep-th].
- [22] F. Pastawski, B. Yoshida, D. Harlow, and J. Preskill, Holographic quantum error-correcting codes: Toy models for the bulk/boundary correspondence, *JHEP* **2015** (6), 1, arXiv:1503.06237 [hep-th].
- [23] M. Van Raamsdonk, Building up space-time with quantum entanglement, *Int J Mod Phys D* **19**, 2429 (2010).
- [24] E. Bianchi and R. C. Myers, On the architecture of spacetime geometry (2014), arXiv:1212.5183 [hep-th].
- [25] J. Maldacena and L. Susskind, Cool horizons for entangled black holes, *Fortschritte der Physik* **61**, 781 (2013), arXiv:1306.0533 [hep-th].
- [26] C. Cao, S. M. Carroll, and S. Michalakis, Space from Hilbert space: Recovering geometry from bulk entanglement, *Phys Rev D* **95** (2017).
- [27] B. Swingle, Spacetime from entanglement, *Ann Rev Cond Matt Phys* **9**, 345 (2018).
- [28] M. Raasakka, Spacetime-free approach to quantum theory and effective spacetime structure, *SIGMA* (2017).
- [29] Notice that since the framework does not have fundamental geometric observables, but the bulk geometry is just an effective description of the boundary correlation structure, the different bulk geometries are not in any sense orthogonal in the Hilbert space, even though some approximate notion of orthogonality may be recoverable in the macroscopic limit.
- [30] We note that the boundary state spaces may be Krein spaces (instead of Hilbert spaces) for a model containing fermionic degrees of freedom [14].
- [31] R. Loll and B. Ruijl, Locally causal dynamical triangulations in two dimensions, *Phys Rev D* **92** (2015).
- [32] K. Huang, *Quantum Field Theory: From Operators to Path Integrals* (Wiley-WHC, 2010).
- [33] P. Virtanen, R. Gommers, T. E. Oliphant, M. Haberland, T. Reddy, D. Cournapeau, E. Burovski, P. Peterson, W. Weckesser, J. Bright, *et al.*, SciPy 1.0: Fundamental Algorithms for Scientific Computing in Python, *Nature Methods* **17**, 261 (2020).
- [34] M. Raasakka, (2025), GitHub repository, address: <https://version.aalto.fi/gitlab/raasakm1/tgravity>.
- [35] Y. Aharonov and D. Bohm, Significance of electromagnetic potentials in the quantum theory, *Phys. Rev.* **115**, 485 (1959).